Parolai, S. (2014): Shear wave quality factor Qs profiling using seismic noise data from microarrays. - *Journal of Seismology*, *18*, 3, p. 695-704.

DOI: http://doi.org/10.1007/s10950-014-9440-5

Shear-wave quality factor Qs profiling using seismic noise data from microarrays

S. Parolai

GFZ German Research Centre for Geosciences, Helmholtzstrasse 7, 14467 Potsdam, Germany. parolai@gfz-potsdam.de

Abstract

The assessment of the shear-wave velocity (Vs) and quality factor (Qs) profiles below a site is necessary to characterize its site response. Recently, methods based on the analysis of seismic noise have proved to be very efficient for providing a sufficiently accurate estimation of the Vs versus depth at reasonable costs for engineering seismology purposes. In this study, it is investigated if the same methods can also provide, with just a few additional and successive calculation steps, realistic Qs versus depth estimations. A data set of seismic noise collected at the Tito test site in southern Italy by a microarray of seismological stations was used, and the obtained Qs results are compared with those estimated by independent geophysical investigations. It is shown that the values are consistent and that the seismic noise analysis has the potential to also provide a more comprehensive (Vs and Qs) description of the geological structure below a site.

Introduction

The reliable assessment of seismic risk at urban scales, which is necessary for effective urban planning and the preparation of rapid response in the case of a disaster, requires a trustworthy assessment of all its main components, namely seismic hazard, seismic vulnerability and exposure.

Seismic hazard assessment at the local scale needs to consider local variations of earthquake-induced ground motion resulting from lateral changes in the near-surface geology (i.e., site effects). Site effects, when earthquake recordings are lacking, can be estimated via numerical simulations once the shear-wave velocity (Vs) and then Quality factor (Qs) below the investigated site are known (Parolai et al., 2012).

In the last decades, several techniques have been proposed for the assessment of the Vs below a site, considering both active (e.g., seismic reflection, borehole investigations) and passive sources. In particular, the latter method, based on the use of seismic noise (e.g., Aki, 1957; Okada, 2003; Parolai et al., 2005; Foti et al., 2011, Boxberger et al., 2011), has several advantages, mainly due to the fact that they are low cost, not invasive, and require short data acquisition times.

On the contrary, the assessment of Qs has attracted less attention, probably due to the difficulties in accurately constraining it from the seismic data. Most of the relevant studies have relied on borehole data (e.g., Assimaki et al., 2006; Parolai et al., 2010) while some attempts have been made using active seismic source generated surface waves (e.g., Xia et al, 2002).

Recently, Prieto et al. (2009) showed that it was possible, at the regional scale, to estimate the attenuation of surface waves using seismic noise recordings. They also inverted for the Qs 1D-structure based on assumptions about the relationship between the shear-wave and primary waves quality factor ratio (Qs/Qp). Similarly, Weemstra et al., (2013) estimated the attenuation and the quality factor of surface waves using recordings from an array with an aperture of several kilometers, but did not attempt any Qs 1D inversions. In terms of more local scales, Albarello and Baliva (2009) estimated the damping in soil by seismic noise measurements, but again did not estimated Qs. Furthermore, none of the above mentioned studies that relied on seismic noise data compared Qs estimations with those derived by independent geophysical investigations.

In this paper, it is shown that it is possible to reliably estimate Qs in the shallow-most geological layers by using seismic noise recordings from microarrays. First, the basis behind the method used for estimating the frequency-dependent attenuation factors is introduced.

Then these are used to derive the quality factor for Rayleigh waves. The basic theory for deriving a 1D Qs velocity profile from the frequency attenuation factors is then introduced, and finally the procedure is applied to the seismic noise data collected by a microarray (maximum interstation distance of the order of a few tens of meters) at the Tito test site (Parolai et al., 2007) where independent Qs estimates are available from borehole earthquake recordings and laboratory analysis.

Method

The space correlation function $\phi(\omega)$ introduced by Aki (1957) is estimated for observed vertical component seismic noise data as (Ohori et al., 2002; Parolai et al., 2007):

$$\phi(\omega) = \frac{\frac{1}{M}\sum_{m=1}^{M} \mathrm{Re}\left({}_{m}S_{jn}(\omega)\right)}{\sqrt{\frac{1}{M}\sum_{m=1}^{M} {}_{m}S_{jj}(\omega) \sum_{m=1}^{M} {}_{m}S_{nn}(\omega)}} \qquad (1)$$

where ${}_{m}S_{jn}$ is the cross-spectrum for the *m*th segment of the seismic noise data, between the *j*th and the *n*th station, M is the total number of used segments, and ω is the angular frequency. The power spectra of the *m*th segment at station *j* and station *n* are ${}_{m}S_{jj}$ and ${}_{m}S_{nn}$, respectively. In an elastic medium, it can be shown that the space correlation function at a certain frequency ω can be described as:

$$\phi(r,\omega) = J_0\left(\frac{\omega}{c(\omega)} r\right) \qquad (2)$$

where J_0 is the zero order Bessel function, $c(\omega)$ is the frequency-dependent Rayleigh wave phase velocity and *r* is the interstation distance.

Prieto et al., (2009) showed that equation (2), in order to take into account attenuation for plane waves, can be modified to be written as:

$$\phi(r,\omega) = J_0\left(\frac{\omega}{c(\omega)} r\right) e^{-\alpha(\omega) r} \qquad (3)$$

$$\alpha(\omega) = \frac{2\pi f}{2 Q_r(\omega) c(\omega)} \qquad (4)$$

where $\alpha(\omega)$ is the frequency dependent Rayleigh wave attenuation factor and $Q_r(\omega)$ is the frequency-dependent quality factor for Rayleigh waves. Recently, Nakahara et al. (2012) and Lawrence et al (2013) demonstrated the validity of this approach from both theoretical and empirical points of view.

Similarly to Parolai et al., (2006), an iterative grid-search procedure can be performed using equation (3) to find the value of the phase velocity $c(\omega)$ and the frequency-dependent attenuation factor $\alpha(\omega)$ that give the best fit to the data. The best fit is achieved by minimizing the root-mean square (rms) of the differences between the values calculated using equations (1) and (3). Data points that differ by more than two standard deviations from the value obtained with the minimum-misfit velocity are removed before the next iteration of the grid search. A maximum of three grid-search iterations are allowed.

Due to the effect of attenuation in shallow geological material, the coherency of the seismic signal is lost after a short propagation distance. In the case that the available data set is dominated by interstation distances much larger than the wavelength of the analyzed frequency, a bias might occur in the estimation of the attenuation factors (the correlation coefficients will simply be randomly scattered around zero). In such a case, it would be advisable to restrict the grid search to interstation distances smaller than a few wavelengths. The tests that we carried out showed that restricting the selection to interstation distances shorter than one and half to two times the wavelength of the signal allows us to obtain stable and robust estimates. That is, important information about the decay with distance of the spatial correlation function is not disregarded and the fit is not biased by the "noisy" large interstation distance data. Note, that in general, the selection of the suggested inter-distance range and the introduction of the exponential function in equation (4), which only acts in modifying the amplitudes of the peaks of the Bessel function, does not affect the estimation of the phase velocity that could be achieved with equation (2). In fact, the phase velocity is determined by the position of the zero-crossing of the Bessel function and only in the case that the maximum interstation distance is much shorter than the wavelength of the analyzed frequency will the Bessel function not show any zero crossing, with different estimates of the phase velocity possibly obtained.

The $Q_r(\omega)$ can then be estimated using equation (4) once the phase velocity and attenuation factor are known. Note, that accordingly to Li (1995) the phase velocity is used in equation (4) and not the group velocity since we are dealing with the spatial quality factor and not with the temporal one.

The relationship between the Rayleigh wave attenuation factor and the quality factor for P- (Qp) and S-waves (Qs) of a layered model is given by (Anderson et al., 1965; Xia et al., 2002):

$$\alpha(\omega) = \frac{\omega}{2c(\omega)^2}\left[\sum_{i=1}^{m} Vpi\,\frac{\partial c(\omega)}{\partial Vpi}\,Qpi^{-1} + \sum_{i=1}^{m} Vsi\,\frac{\partial c(\omega)}{\partial Vsi}\,Qsi^{-1}\right] \qquad (5)$$

where Qpi and Qsi are the quality factors for P- and S-waves of the i*th l*ayer, respectively; Vpi and Vsi are the P- and the S-wave velocities of the i*th* layer, respectively and *m* is the number of layers of a layered earth model.

Equation (5), when the attenuation factors for several frequencies are considered, is a linear system in the form:

$$\mathbf{Ax} = \mathbf{d} \qquad (6)$$

where **x** is the model vector containing the inverse of the quality factors Qpi^{-1} and Qsi^{-1}, **d** is the data vector whose elements are the attenuation factors $\alpha(\omega)$ and **A** is the data kernel matrix with elements $\frac{\omega}{2c(\omega)^2} Vpi \frac{\partial c(\omega)}{\partial Vpi}$ and $\frac{\omega}{2c(\omega)^2} Vsi \frac{\partial c(\omega)}{\partial Vsi}$ determined by (5). Since the quality factors can only assume positive values, the system is solved using a least squares algorithm employing a positivity constraint (e.g., Menke, 1989). Furthermore in order to mitigate the influence of errors in the data a damping factor is introduced and equation (6) takes the form:

$$\begin{pmatrix} \mathbf{A} \\ \lambda \mathbf{I} \end{pmatrix} \mathbf{x} = \begin{pmatrix} \mathbf{d} \\ \mathbf{0} \end{pmatrix} \qquad (7)$$

where **I** is the identity matrix, λ is the damping factor and **0** a vector containing zeroes.

In general, when Vs/Vp is larger than 0.4, the attenuation factor dependence on Qp is significant and therefore Qp can also be estimated (Xia et al., 2002). In all other cases, the inversion can be carried out only for Qs. In these cases, equation (5) becomes:

$$\alpha(\omega) = \frac{\omega}{2c(\omega)^2} \left[\sum_{i=1}^{m} Vsi \frac{\partial c(\omega)}{\partial Vsi} Qsi^{-1} \right] \qquad (8)$$

The Tito test site

The Tito test site is located in the Saint Loja Plain in southern Italy. A borehole of 40 m depth was drilled down to the engineering bedrock and a seismometer was installed at 35 m depth. The water level was encountered just few meters below the surface. During the drilling, undisturbed samples were taken and subjected to geotechnical testing (Parolai et al., 2007). In addition, S-wave velocities were estimated by standard downhole measurements that have been used by Parolai et al., (2007) to derive an S-wave velocity profile and Qs. Parolai et al., (2007) also carried out seismic noise measurements using micro arrays. Furthermore, using earthquake recordings, Mucciarelli and Gallipoli (2006) estimated the Qs in the uppermost 35 m by a nonparametric damping analysis.

This site was therefore chosen for the application of the proposed approach due to the availability of independent data. The seismic noise recordings considered were collected by array 1 of Parolai et al., (2007). This array consisted of 11 seismological stations deployed following an irregular geometry. The stations operated simultaneously for more than 1 hour, recording noise at 500 samples/sec. Each station was equipped with a 24 bit digitizer connected to a Mark L-4C-3D 1 Hz sensor and a Global Position System (GPS) timing. For the analysis required to obtain the spatial correlation coefficients of equation (1), each station's data were divided into 60 second windows. More information about the geological nature of the site and the analysis carried out can be found in Parolai et al., (2007).

The S-wave velocity profile estimated by Parolai et al. (2007) for this array reaches several hundred meters depth. However, since the independent Qs estimates are available only for the uppermost 35 m, I restrict my analysis to the frequency range 3.25 Hz-10.64 Hz, that when considering the estimated phase velocities, limits the depth of investigation to the uppermost 35 m and allows spatial aliasing problems to be avoided.

Results

Attenuation factors estimation

The results of the grid search procedure for 3 analyzed frequencies are shown in Figure 1. These frequencies have been chosen to show the results at the extremes and the center of the analyzed frequency range. In the grid search procedure, $c(\omega)$ was varied between 50 and 3000 m/sec in steps of 1 m/sec in order to exhaustively cover all possible values that the Rayleigh wave phase velocity might assume, while $\alpha(\omega)$ was varied between 0 and 0.0598 (m^{-1}) in steps of 0.0002 m^{-1}. In Figure 1, for sake of readability, the results are shown over the 50 and 1000 m/sec velocity range. Since in our data set few interstation distances are larger than one and half to two times the wavelength (for the latter, only for the highest frequencies we analyze), we did not apply any selection criteria during the grid search, apart that based on the rms threshold. Tests we carried out showed that this choice has no influence on the final results.

It is clear, since the error functions show a very narrow minimum along the velocity axis and is only smeared along the α axis, that the phase velocity is very well constrained and the values are the same as those obtained using equation (2) ($\alpha(\omega)$ equal to 0 corresponding to the elastic case). This is also confirmed by the fact that the minimum misfit functions obtained by equations (2) and (4) share the same zero crossing value on the x axis (Figure 2). The attenuation factors can be fairly well constrained, although the uncertainty increases with increasing frequency. Note that for the highest frequency (10.16 Hz) presented in Figure 1, the normalized fit value decreases by 5% from that obtained by the best fitting $\alpha(\omega)$ to that estimated by considering the maximum $\alpha(\omega)$ value tested in the grid search (0.0598).

Figure 2 shows the fitting of the data for the same frequencies presented in Figure 1 when using equations (2) and (3). The improvement in the fit of the data obtained when considering the attenuation factor is not only visual, but it is confirmed, for example, for the frequencies shown in Figures 1 and 2, by a rms reduction of 25%, 3,8% and 25%, respectively. The general improved data fit when using equation (3) can be better appreciated in Figure 3 where all the considered frequency and distances couples are shown.

The estimated attenuation factors are depicted in Figure 4a while Figure 4b shows the $Q_r(\omega)$ and Figure 4c the dispersion curve derived through equation (4). Note that the dispersion curve is identical to that used in Parolai et al., (2007) and shown in their Figure 7. In general, a trend for $\alpha(\omega)$ to increase with frequency is seen. This was expected considering equation (4) within the frequency band where the dispersion curve becomes nearly flat (above 5 Hz in the case at hand).

However, at lower frequencies, a more complicated frequency dependence of $\alpha(\omega)$ is observed. Since the dispersion curve is showing a typical smooth increase of velocity towards lower frequencies (from 5 Hz down to the considered 3.25 Hz in Figure 4c), this trend is mainly related to the variation of $Q_r(\omega)$ (Figure 4b). This behavior hints at a variation with depth of the quality factor. The $Q_r(\omega)$ generally gives values of 5, but between 5 Hz and 6 Hz, it increases to up to 15. This is consistent with the smaller misfit reductions obtained while using equation (3) instead of equation (2) (elastic case) for the frequency shown in the central panel of Figure 2 (5.61 Hz) with respect to the other two (i.e., 3.25 Hz and 10.16 Hz). In fact, the results of equations (2) and (3) tend to become more similar when Q is higher.

Quality factor inversion

The attenuation factor inversion we propose in this study should follow the dispersion curve inversion generally carried out for estimating the shear- wave velocity profile. In this study, in order to estimate the body-wave quality factor, the 1D-structure S-wave velocity model already derived by Parolai et al. (2007) for the same data set was considered. In this model, the uppermost 35 m are made up of 5 layers (Table). First, the data kernel matrix **A** considering both the P- and the S-wave velocity contribution to the attenuation factors (equation (5)) was estimated. As it might be expected for a medium where the Vs/Vp ratio is much smaller than 0.4 (see Table 1), the contribution of Vp to the attenuation factor is negligible (as shown for the analyzed case in Figure 5, by small elements of the data kernel matrix corresponding to the Qp calculated by using equation (5)). Therefore, the inversion was carried out using equation (8), which only accounts for the contribution of Vs and Qs.

In this case the system of equation (8) becomes

$$\begin{bmatrix} \frac{\omega 1}{2c(\omega 1)^2} Vs1 \frac{\partial c(\omega 1)}{\partial Vs1} & . & . & . & . & \frac{\omega 1}{2c(\omega 1)^2} Vsm \frac{\partial c(\omega 1)}{\partial Vsm} \\ . & & & & & . \\ . & & & & & . \\ . & & & & & . \\ \frac{\omega n}{2c(\omega n)^2} Vs1 \frac{\partial c(\omega n)}{\partial Vs1} & . & . & . & . & \frac{\omega n}{2c(\omega n)^2} Vsm \frac{\partial c(\omega n)}{\partial Vsm} \\ \lambda 1 & & & & & \\ & & . & & & \\ & & & . & & \\ & & & & & \lambda m \end{bmatrix} \cdot \begin{bmatrix} Qs1^{-1} \\ . \\ . \\ Qsm^{-1} \end{bmatrix} = \begin{bmatrix} \alpha(\omega 1) \\ . \\ . \\ . \\ . \\ . \\ \alpha(\omega n) \\ 0_1 \\ . \\ 0_m \end{bmatrix} \qquad (9)$$

where m =5 is the number of layers of the model and n =27 is the number of attenuation factors used (sufficient selected number of frequencies from the original data set that are able describe the trend in the attenuation factor curve). The value of the damping factor λ was fixed after a series of test inversions (a value of 0.1 was adopted), allowing the rms differences between the observed and calculated (using the inversion results) attenuation factors to be minimized but still providing physically acceptable solutions.

The final values obtained for Qs are 9.8, 11.2, 50.1, 13.9, and 7.7, for the first, second, third, fourth and fifth layer, respectively. These values, as expected considering equation (5), are larger than those obtained for Q_r. Figure 3a shows that the attenuation factors retrieved with the inversion model fairly closely describe the observed data. A better data fitting might be possible by increasing the number of layers, however, this would involve the risk of over-fitting the data.

Discussions and conclusions

The Qs values obtained for the uppermost 35 m at the Tito test site are low, but generally consistent with those observed in soft sedimentary layers (e.g., Parolai et al., 2010). In order to assess if they are realistic for the site at hand, they were compared to the values obtained for the same site by Parolai et al., (2007) using downhole active seismic recordings and Mucciarelli and Gallipoli (2006) who used earthquake data.

To carry out the comparison, the average quality factor of the uppermost 35 m Qs_{tot} was calculated by using:

$$\frac{t_{tot}}{Qs_{tot}} = \sum_{i=1}^{m} \frac{ti}{Qsi} \tag{10}$$

$$t_{tot} = \sum_{i=1}^{m} ti \tag{11}$$

where ti is the travel time in each layer i, t_{tot} is the total travel time, and Qsi is the quality factor in each layer.

A Qs_{tot}=12.5 was obtained, which is in good agreement with the estimates of Mucciarelli and Gallipoli (2006) who derived Qs values ranging between 15 and 30.

Parolai et al., (2007) calculated frequency dependent Qs over the frequency range 30 Hz-80 Hz. Qs was estimated to increase with frequency from 6 to 30,(with these larger values being affected by larger uncertainties due to a lower signal-to-noise ratio at high frequencies) again in good agreement with the value derived in this study.

Furthermore, the estimated average Qs value is in good agreement with the results of Parolai et al. (2007) (see their Figure 16) which found that the best fit of the synthetic surface-to-borehole spectral ratio to the empirical one was obtained when using a Qs value of 10. In addition, the numerical simulations carried out to estimate the synthetic surface-to-borehole spectral ratio using the model derived in this study confirmed the results of Parolai et al. (2007) and therefore are not shown here.

The large jump in the Qs factor to a value of 50 in the third layer might be related to a weakly constrained solution for Qs in this layer (see the small elements of the data kernel matrix corresponding to it in Figure 5). In order to estimate the influence of such a sudden change in the Qs structure on wave propagation, we carried out numerical simulations of vertical propagating S-waves using a semi-analytical method (Wang, 1999), one using the Qs structure estimated in this paper, and one replacing in the third layer the Qs value of 50.1 with a value of 10 (Parolai et al., 2007) and calculating seismograms for the surface and a depth of 35 m. The results, shown in Figure 6, show that the effect is minimal, as well as demonstrating that it is the average Qs along the depth profile that mainly dominates the attenuation of seismic waves in the uppermost 35 m in the frequency band of interest.

It is therefore believed that the analysis of seismic noise data can provide reliable estimates of the Qs below a site that might be used for engineering seismology purposes. This means that by adopting the same techniques of acquisition and data analysis used for estimating the shear wave velocity profile, but adding a few additional calculation steps, it is possible to have a comprehensive (from an engineering seismology point of view) description of the shallow subsoil structure. This would make it possible characterize a site at a low cost using a non-invasive methods, allowing site effects investigations to cover large urban areas with a high spatial resolution. The benefit for seismic hazard assessment, especially in urban areas built in very heterogeneous geological environments is obvious. The method adopted here should be further tested in other sites with different mechanical properties of the shallow geology layers (Vs, Vs/Vp ratio etc.), but where independent estimates of the quality factor are available. In particular, in this study, the existence of a shallow water table at the analyzed site made it impossible to evaluate the proposed approach for estimating Qp.

Future work will also consider the possibility of applying the proposed method, with a few modifications, to the analysis of data collected in buildings and by arrays installed above laterally heterogeneous structures.

Data and resources

Data used in this study were collected in the framework of a scientific cooperation between the GFZ German Research Centre for Geosciences, the Universita’ della Basilicata and the CNR-IMAA who run the Tito test site.

Acknowledgements

I thank D. Bindi, M. Pilz and K. Fleming for very constructive discussions and suggestions.
I thank Marco Mucciarelli for comments and suggestions that helped in improving the manuscript. K. Fleming kindly improved the English.

References

Aki, K. (1957). Space and time spectra of stationary stochastic waves, with special reference to microtremors. Bulletin of the Earthquake Research Institute 35, 415–456.

Albarello D. and Baliva F. (2009). In-situ estimates of material damping from environmental noise measurements. Mucciarelli, Marco; Herak, Marijan; Cassidy, John (Eds.), Increasing Seismic Safety by Combining Engineering Technologies and Seismological Data (NATO Science for Peace and Security Series C: Environmental), Springer, XVIII, 382 pp., ISBN: 978-1-4020-9194-0, 73-84.

Anderson D.L., Ben-Menahem A., Archambeau C.B. (1965). Attenuation of seismic energy in the upper mantle. J. Geophys. Res. 70, 1441-1448.

Assimaki D., Steidl J., Liu P.C. (2006). Attenuation and velocity structure for site response analyses via downhole seismogram inversion. Pure and Appl. Geophys.163, 81-118.

Boxberger, T., Picozzi, M., Parolai, S. (2011). Shallow geology characterization using Rayleigh and love wave dispersion curves derived by seismic noise array measurements. Journal of Applied Geophysics, 75, 2, 345-354.

Foti, S., Parolai, S., Albarello, D., Picozzi M. (2011). Application of Surface-Wave Methods for Seismic Site Characterization. Surveys in Geophysics, 32, 6, 777-825.

Lawrence, J.F., Denolle M., Seats K.J., Prieto G. (2013). A numerical evaluation of attenuation from ambient noise correlation functions. J. Geophys. Res. Solid Earth, 118, 6134-6145, doi:10.1002/2012JB009513.

Li X.-P. (1995). Attenuation dispersion of Love waves in a two-layered half space. Wave Motion, 22, 349-370.

Menke,W. (1989) Geophysical data analysis: Discrete inverse theory, Academic Press,322 ISBN0-12-490921-3

Mucciarelli, M., and Gallipoli M.R. (2006). Estimate of frequency and damping for large set of buildings in dense urban areas, Presented at First European Conference on Earthquake Engineering and seismology, Geneva, Switzerland, 3–8 September 2006, paper no. 211.

Nakahara H., (2012). Formulation of the spatial autocorrelation (SPAC) method in dissipative media. Geophys. J. Int., 190, 1777-1783, doi:10.1111/j.1365-246X.2012.05591.x

Ohori, M., Nobata, A., Wakamatsu, K. (2002). A comparison of ESAC and FK methods of estimating phase velocity using arbitrarily shaped microtremor analysis, Bull. Seism. Soc. Am., 92, 2323-2332.

Okada, H. (2003). The Microtremor Survey Method. Geophysical monograph series 12

Parolai, S., Picozzi, M, Richwalski S.M., Milkereit (2005). Joint inversion of phase velocity dispersion and H/V ratio curves from seismic noise recordings using a genetic algorithm, considering higher modes. Geoph. Res. Lett.32, L01303, doi: 10.1029/2004GL021115.

Parolai, S., Richwalski, S.M., Milkereit, C., Faeh, D. (2006). S-wave velocity profile for earthquake engineering purposes for the Cologne area (Germany), Bull. Earthq. Eng., 65-94, doi:10.1007/s10518-005-5758-2.

Parolai, S., Mucciarelli, M., Gallipoli, M.R., Richwalski, S.M., Strollo, S. (2007). Comparison of Empirical and Numerical Site Responses at the Tito Test Site, Southern Italy, Bull. Seism. Soc. Am., 97, 1413-1431.

Parolai, S., Bindi, D., Ansal, A., Kurtulus, A., Strollo, A., Zschau, J. (2010). Determination of shallow S-wave attenuation by down-hole waveform deconvolution: a case study in Istanbul (Turkey). - Geophysical Journal International, 181, 2, 1147-1158

Parolai, S. (2012). Investigation of site response in urban areas by using earthquake data and seismic noise. - In: Bormann, P. (Eds.), New Manual of Seismological Observatory Practice 2 (NMSOP-2), 1-38.

Prieto, G.A, Lawrence J.F., Beroza G.C. (2009). Anelastic earth structure from the coherency of the ambient seismic field. J. Geophys. Res. 114, B07303, doi:10.1029/2008JB006067

Wang, R. (1999). A simple orthonormalization method for stable and efficient computation of Green's functions, Bull. Seism. Soc. Am., (83), 733-741.

Weemstra C., Boschi L., Goertz A., Artman B. (2013). Seismic attenuation from recordings of ambient noise. Geophysics, 78, P.Q1-Q14, doi:10.1190/GEO2012-0132.1

Xia, J., Miller, R.D., Park, C.B., Tian, G. (2002). Determining Q of near-surface materials from Rayleigh waves. Journal of Applied Geophysics, 51, 121-129

Figure Captions

Figure 1: The normalized fit value (estimated as rms_{min}/rms) over the area of a grid search. White triangles indicate the $\alpha(\omega)$ and $c(\omega)$ combination that provide the best fit to the observed spatial correlation coefficients.

Figure 2: Measured space-correlation function values (black dots) for the same frequencies as in Figure 1 at the Tito test site, and the best-fitting functions given by equations (2) (dashed gray line) and (3) (solid gray line). Gray dots indicate the space-correlation values discarded by the fitting procedure.

Figure 3: :Spatial correlation coefficients from observed data (top left), from the grid search using equation (3) (top right) and from the grid search using equation (2) (bottom).

Figure 4: a) Observed attenuation factors (black circles) and retrieved attenuation factor after the inversion (gray circles). b) Rayleigh wave quality factor Q_r. c) Rayleigh wave phase velocities.

Figure 5: The data kernel matrix determined using equation 5 (see the main text). The elements corresponding to the first 5 rows are related to the dependence of the attenuation on the Vp velocity. The elements from row 5 to 10 are related to the dependence of the attenuation on Vs.

Figure 6: Synthetic S-wave seismograms calculated at the surface and a depth of 35 m considering the model described in Table 1 and the Qs structure estimated in this study (gray continuous line) and replacing in the third layer the value of 50.1 with 10 for Qs (black dashed line).

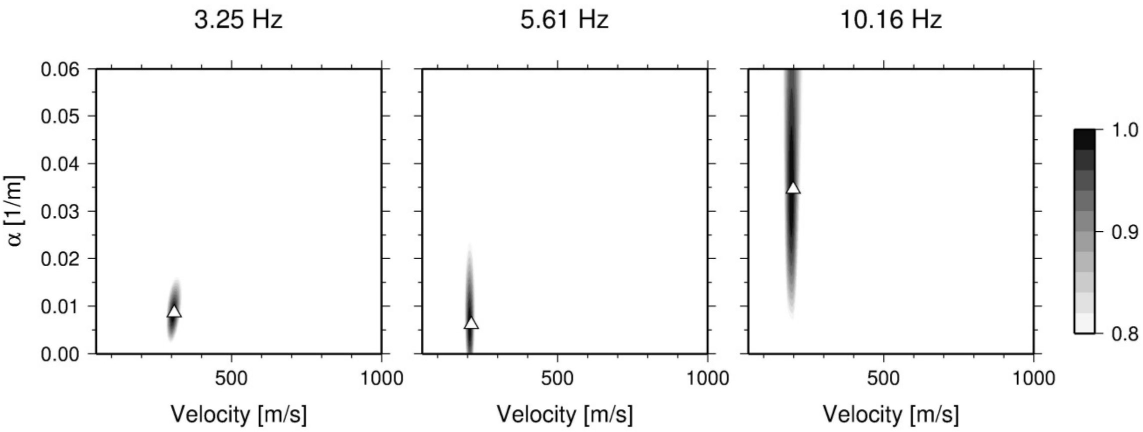

Figure 1: The normalized fit value (estimated as rms_{min}/rms) over the area of a grid search. White triangles indicate the $\alpha(\omega)$ and $c(\omega)$ combination that provide the best fit to the observed spatial correlation coefficients.

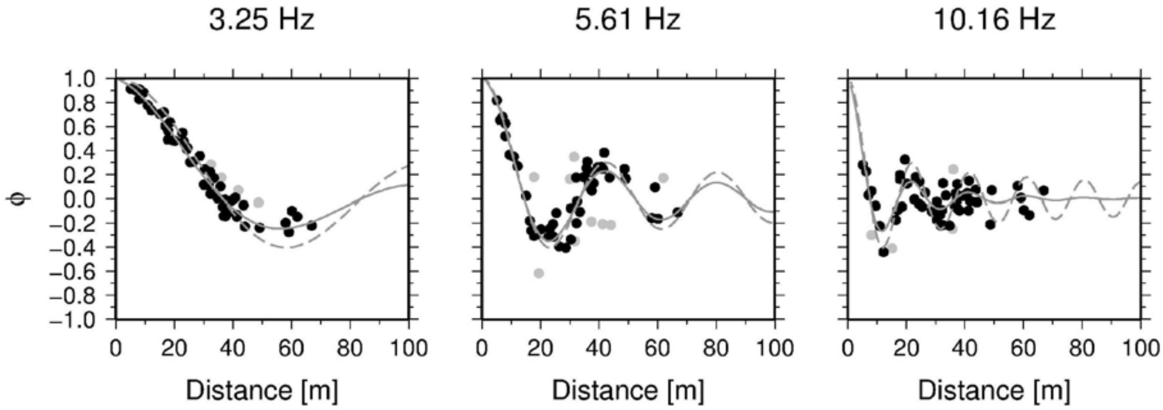

Figure 2: Measured space-correlation function values (black dots) for the same frequencies as in Figure 1at the Tito test site, and the best-fitting functions given by equations (2) (dashed gray line) and (3) (solid gray line). Gray dots indicate the space-correlation values discarded by the fitting procedure.

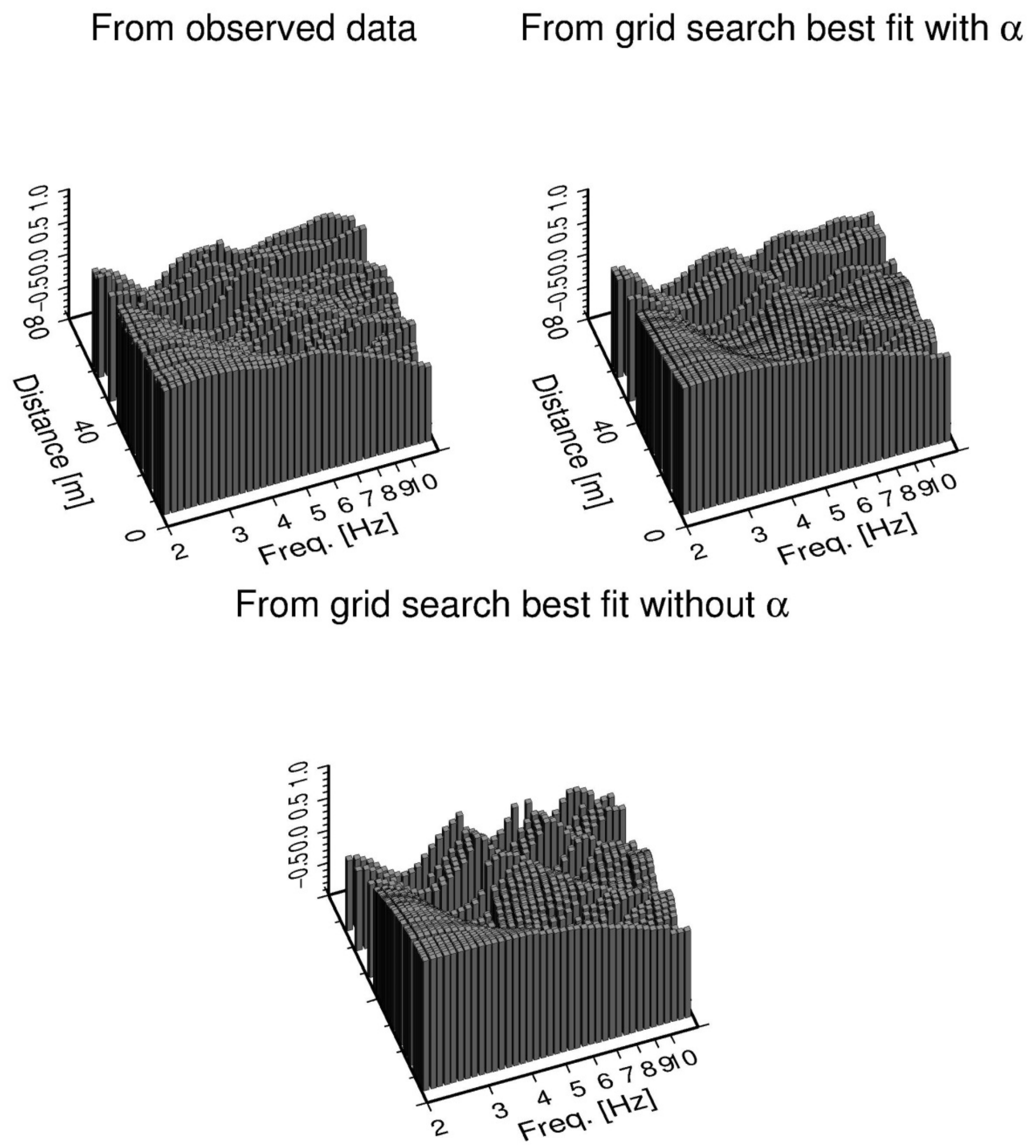

Figure 3: Spatial correlation coefficients from observed data (top left), from the grid search using equation (3) (top right) and from the grid search using equation (2) (bottom).

a) b) c)

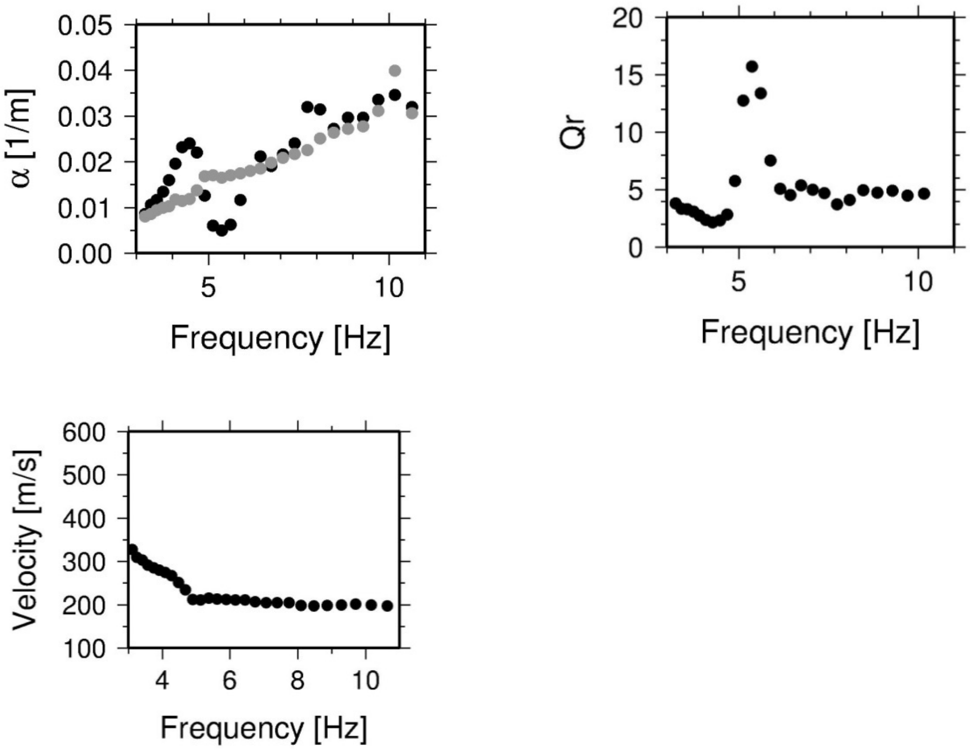

Figure 4: a) Observed attenuation factors (black circles) and retrieved attenuation factor after the inversion (gray circles). b) Rayleigh wave quality factor Q_r. c) Rayleigh wave phase velocities.

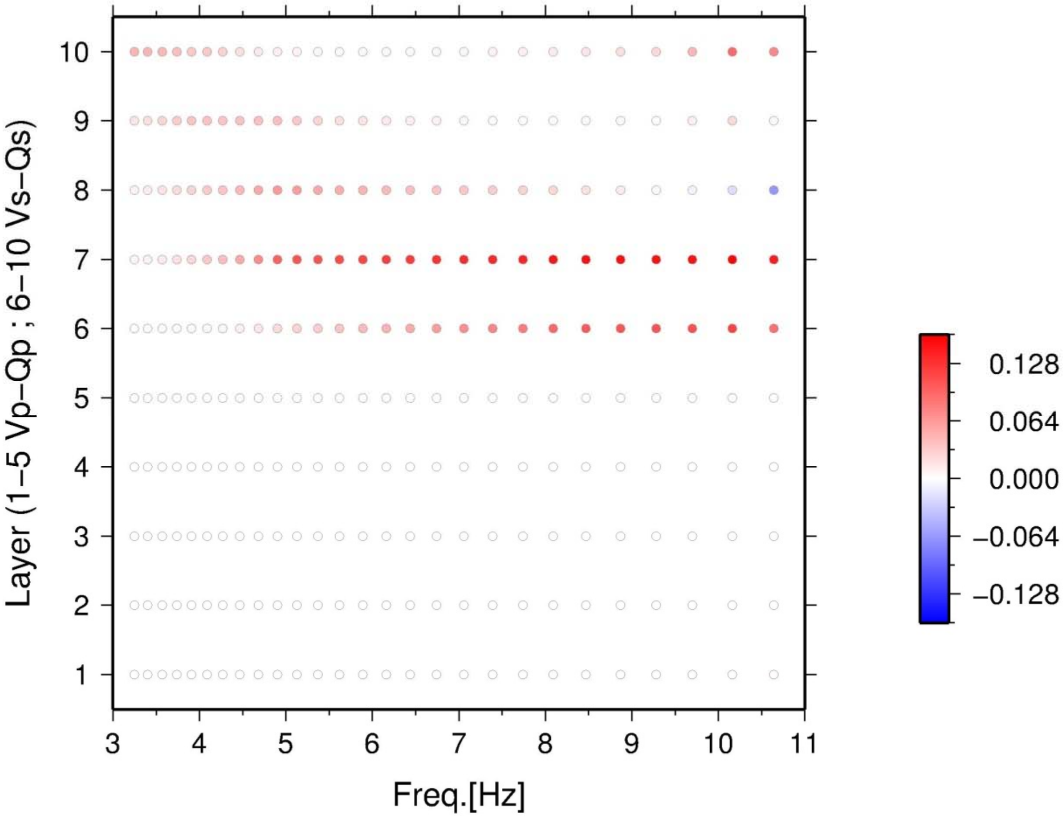

Figure 5: The data kernel matrix determined using equation 5 (see the main text). The elements corresponding to the first 5 rows are related to the dependence of the attenuation on the Vp velocity. The elements from row 5 to 10 are related to the dependence of the attenuation on Vs.

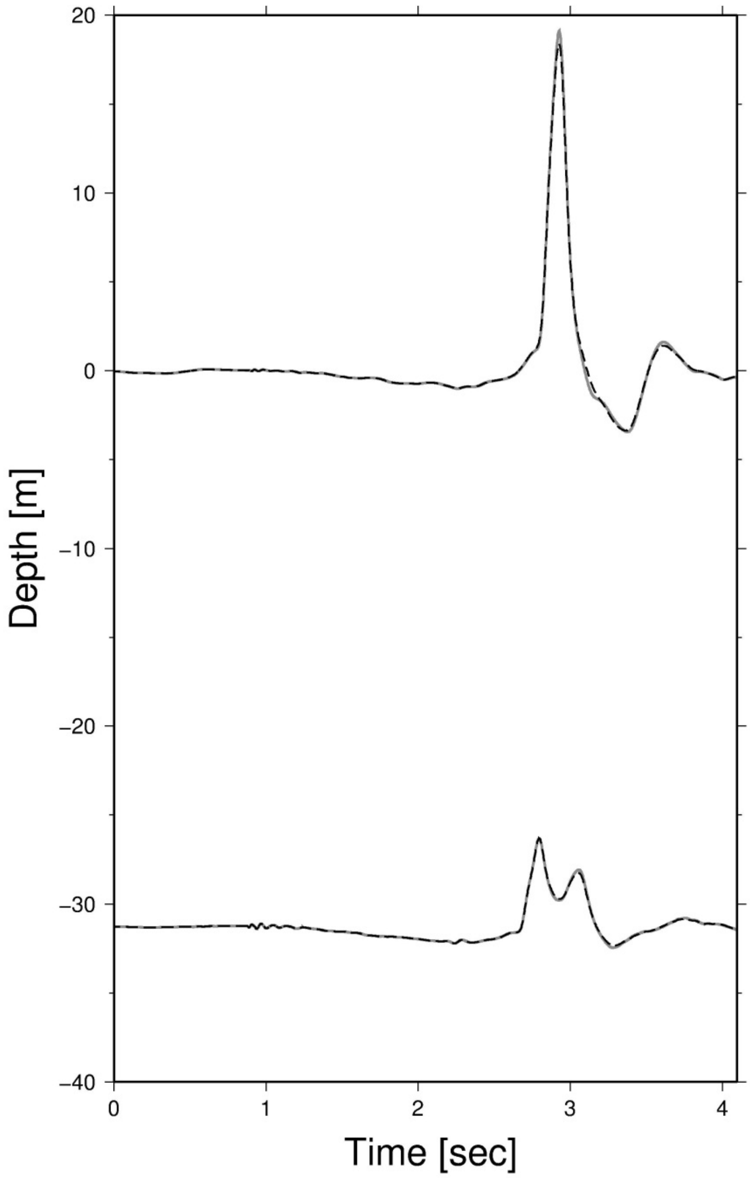

Figure 6: Synthetic S-wave seismograms calculated at the surface and a depth of 35 m considering the model described in Table 1 and the Qs structure estimated in this study (gray continuous line) and replacing in the third layer the value of 50.1 with 10 for Qs (black dashed line).

Table 1: 1D model used for the quality factor inversion. The first column shows the shear-wave velocity, the second column the thickness of the layer, the third column the density and the fourth column the P-wave velocity.

Vs (m/s)	H(m)	ρ kg/m^3	Vp (m/s)
202	6.9	1800	1514
190	8.5	1900	1501
212	5.4	1900	1525
310	10.4	1900	1600
324		2000	1650